sciendo

Structural, optical and vibrational study of zinc copper ferrite nanocomposite prepared by exploding wire technique

SURENDRA SINGH[1], ANSHUMAN SAHAI[2], S.C. KATYAL[1], NAVENDU GOSWAMI[1,*]

[1]Department of Physics and Materials Science and Engineering, Jaypee Institute of Information Technology,
A-10, Sector-62, Noida-201307, India

[2]Department of Physics, Manav Rachna University, Sector-43, Aravalli Hills, Delhi Surajkund Road, Faridabad-121004, India

We have synthesized zinc-copper ferrite (ZCFO) employing exploding wire technique (EWT). The X-ray diffraction (XRD) data confirm the formation of single phase spinel ZCFO, which is in good agreement with Fourier transform infrared spectroscopy (FT-IR), UV-Vis, and Raman spectroscopic analyses. It is also clearly seen in the SEM micrographs that the grains in ZCFO ferrite are very rough, which allows adsorption of gas like oxygen and therefore, the material can behave as active sensing surface. The size range of the grains in prepared sample is of 200 nm to 500 nm. The FT-IR spectrum of the nanocomposite consists of two broad bands, one at 580.4 cm^{-1} due to M–O stretching mode at the tetrahedral site and the other at 400.7 cm^{-1} due to M–O stretching mode at the octahedral site. The nanoparticles show a UV-Vis absorption band in the wavelength region of 400 nm to 700 nm. The energy band gap for the prepared nanomaterial was estimated to be 3.16 eV. Thus, the ferrite nanocomposite prepared by EWT is optically active. According to present literature, Raman spectroscopy study on zinc-copper ferrite system has not been reported till date. By suitable attributing various Raman modes, we have further confirmed the formation of ZCFO nanophase through the present novel approach.

Keywords: *ferrites; explosion; exploding wires; nanoparticles; nanotechnology*

1. Introduction

Ferrites are significant magnetic materials especially for electromagnetic wave band applications due to their unique magnetic and dielectric properties [1]. They are considered as the most versatile high-tech materials because of their extensive applications in radar, microwave communication, magnetic recording and computer memories [2]. Ferrites are reported as excellent absorbers of stray electromagnetic signals [3]. There is a remarkable improvement in the properties of ferrites at nanoscale dimensions and this motivated us to synthesize and investigate the nanoscale spinel ferrite. The field of magnetic nanoferrites attracts worldwide interest of researchers owing to their unique electronic, optical and magnetic properties which could be tuned through external magnetic field, hence, opening new possibilities from technological and theoretical point of view [4–6].

Previous studies on nanoferrites could establish that there is an increase in coercivity H_c, and significant reduction in the saturation magnetization M_s on moving from bulk to nanoscale [7, 8]. At nanoscale dimensions, the rate of chemical reaction is significantly enhanced due to small particle size, large number of coordination sites, and high surface to volume ratio [9]. Owing to this, reactive nanoparticles are widely used in different fields of applications. At nanoscale dimensions, the ionic radii of a cation decide its position in the lattice, especially in the case of doping and compounds having more than one cation [10]. Catalytic and magnetic properties of nanoparticles of spinel ferrites containing transition metal are different from their bulk counterparts, therefore, they find applications in magnetic resonance imaging, magnetic memory devices, photo-magnetic materials, and target-specific drug delivery systems [11]. The improvement in the properties of nanoferrites led to a wide range of novel applications in medical science for diagnostics and cancer therapy,

---

*E-mail: navendugoswami@gmail.com

magnetic drug delivery, gas sensing, superparamagnetic, photocatalyst and high-density information storage devices [12].

Spinel ferrites become more relevant for applications as they are chemically inert and their properties could be tuned via chemical processes [8]. The space group and general formula of spinel ferrite is Fd3m and MFe_2O_4, respectively, where M stands for divalent metal ions of Cu, Zn, Mn, Co, Ni, etc. The unit cell consists of 56 ions, out of which 32 oxygen anions are distributed in closed packed cubic structure and 24 cations occupy tetrahedral sites (A-sites) and octahedral sites (B-sites). Here, 8 out of 64 available tetrahedral sites (A-sites) and 16 out of 32 available octahedral sites (B-sites) are filled by 24 cations. The outstanding optical, magnetic, catalytic, and electrical properties of nanoferrites have been motivating the researchers to investigate them in depth.

The spinel ferrites are different from conventional metal oxide semiconductors in the sense that the conductivity type and resistance can be controlled by changing cation positions [13]. In the structural formula of the spinel compound $(M_{1-i}Fe_i)^A(M_iFe_{2-i})^BO_4$, the expressions in brackets represent the occupancy of A-sites and B-sites and i stands for inversion parameter [14]. The spinel structure can be normal, inverse or partially inverse on the basis of cation distribution between A-sites and B-sites [15]. The normal spinel ferrite (i = 0) has 8 divalent cations at tetrahedral sites and 16 trivalent cations at octahedral sites [15]. The inverse spinel ferrite (i = 1) has 8 trivalent cations at tetrahedral sites and 16 cations at octahedral sites, out of which 8 cations are divalent and remaining 8 cations are trivalent [15]. The partially inverse spinel ferrite (0 < i < 1) has bivalent cations at both sites [15]. Thus, the properties of ferrites can be tailored by positioning cations between A-sites and B-sites. The electronic configuration and ionic valency have significant influence on the cation distribution [15]. Nanoscale ferrites of binary transition metals such as Zn–Ni, Zn–Mn, etc., have been reported as catalysts for alkylation of aromatics, used

commercially as base material for drugs and chemicals [9, 16–18]. Owing to superior magnetic properties of Zn–Mn- and Ni–Zn-based spinel nanoferrites, they are potential material for magnetic cores of read-write head for recording [19]. Banerjee et al. [9] have reported on catalytic performance of nanocrystalline Zn–Cu ferrite (ZCFO) for alkylation of pyridine. Jain et al. [10] have reported ZCFO nanoparticles as LPG sensing agent. Lopez et al. [2] have reported Co–Zn ferrite NP as a soft magnetic material showing super-paramagnetic behavior at room temperature.

It is noteworthy that physical, magnetic, and electrical properties of ferrites having the same composition but prepared by different techniques, are different [12]. According to previous studies on spinel ferrites, different synthesizing techniques, such as mechanical ball milling method [20], co-precipitation method, sol-gel method [21], hydrothermal synthesis method, etc., have been widely adopted till now. In this paper, we have adopted a novel method of exploding wire technique (EWT) [22–26]. The method of EWT was previously reported for synthesis of nanoferrites for a large scale production of pure phase semiconductor nanoparticles [3, 22–26]. A meticulous synthesis and characterization of water driven stable metal sulfide nanoparticles of Zn and Cd were also reported by Goswami et al. [24, 26] employing EWT method. Recently, the method of EWT was successfully extended for the synthesis of copper oxides nanoparticles [25]. According to present literature survey, no report is available up to now for the synthesis of ferrites nanoparticles employing EWT. Here, we explore EWT to obtain ZCFO nanoparticles. The nanoparticles obtained by EWT were characterized in terms of their structural, optical, electronic and vibrational properties.

2. Experimental

2.1. Synthesis

EWT has been employed earlier to synthesize nanoparticles of different materials [22–24]. In this method, a high density impulse current of the order of 10^4 A/mm^2 to 10^6 A/mm^2 is passed through

1 mm diameter zinc wire. Due to high injection rate of energy in the wire, the process of expansion of the heated material is delayed as compared to the rate of change of energy density; therefore as a result, the wire material explodes [24]. The theory of changes in electrodynamics in wire/plate can be explained as follows: during the increase of exploding current, imbalance of self-induced electromotive forces and ohmic potential causes rapture and, consequently, segmentation of the wire [27]. An axial force is developed on the circuit element because of mutual action of current. The force F is $I^2\log(L/D)$ where I stands for current [A], L and D, respectively, denote length and diameter of the wire. This axial force exists between conducting wire and the induced field medium of conductor [28]. The sudden build-up of current causes rapture in conductor but insufficient to separate electrons [28]. Thus, the conductor fragments into smaller size nanoparticles [28]. To practically implement the EWT, high density of current must be maintained so that the voltage-current relation became nonlinear [28]. The diameter of the wire at the point of contact with metal plate during the explosion (called z-pinch) must be very small relative to the rest of the conductor to maintain extremely high current density [22]. This is a basic requirement for explosion to take place and every time a contact between the wire and the plate is made and broken. Lastly, there must be a medium in which the explosion takes place.

For synthesis, zinc wire (diameter: 1.0 mm, purity: 99.5 %) and copper plate (50 mm × 50 mm, thickness: 4.76 mm, purity: 99.95 %) were procured from Goodfellow Cambridge Ltd., UK. Ferric oxide in powder form (purity: 99.99 %) was used as supplied by Sigma-Aldrich manufactures. A battery (12 V, 80 Ah) was utilized as a source of power supply.

The synthesis procedure is as follows. The copper plate (mass 46.46 g) was dipped in 2 L aqueous solution of Fe_2O_3 (Fig. 1). The solution was continuously agitated using magnetic stirrer. Copper plate and zinc wire were connected to the negative and positive terminals of 12 V battery, respectively. The Zn wire was struck against the plate inside
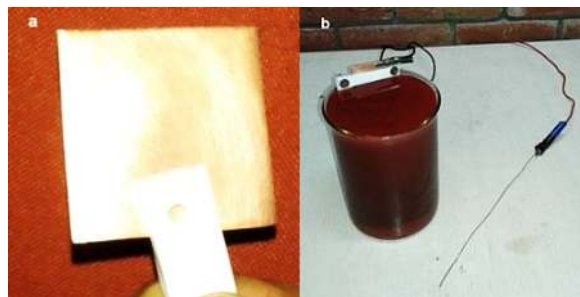

Fig. 1. (a) 99.95 % pure copper sheet; (b) setup showing Cu plate immersed in aqueous solution of Fe_2O_3, connected to one terminal of battery and Zn wire connected to the other terminal.

the aqueous medium in such a way that the wire landed on the plate surface at 90°. Sparking produced at each strike gave rise to nanofragments of Cu and Zn which, subsequently, combined with Fe_2O_3 to form a nanocomposite sample of ZCFO. After exploding Zn wire against Cu plate in the aqueous solution of Fe_2O_3, a colloidal suspension was obtained. Now, water was decanted and the sediment was dried. Finally, fine powder form of nanomaterial sample was obtained by grinding the dry sediment. The explosion of 22.74 g of Zn wire against a 5 mm thick Cu plate dipped in the 2 L aqueous solution containing 27 g of ferric oxide caused erosion of Cu plate by 15.13 g and, finally, 43.7 g of nanosized powder form of ZCFO was yielded.

2.2. Characterization

Several characterization techniques were employed to investigate the prepared nanomaterials. We performed XRD analysis with CuKα ($\lambda = 1.54056$ Å) as radiation source in the present work to determine the crystalline phase of the prepared material [24]. Scanning electron microscope with accelerating voltage in the range of 5 kV to 30 kV was used for microstructural characterization of the sample. Fourier transform infrared (FT-IR) spectrophotometer was used in the range of 370 cm^{-1} to 4000 cm^{-1} to probe the IR active vibrational modes. The FT-IR spectrum was acquired for the nanopowder mixed with KBr and then pelletized at a pressure of 1.33×10^3 Pa/min. UV-Vis
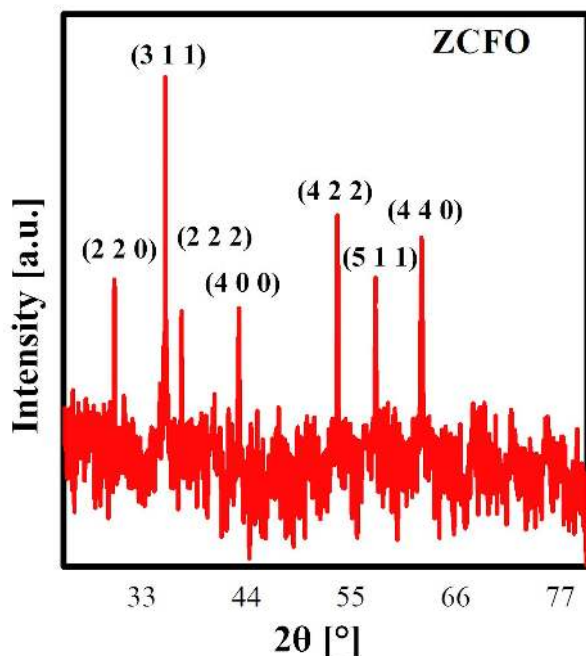
Fig. 2. XRD spectrum of the prepared nanomaterial zinc-copper ferrite (ZCFO).

spectrophotometer, allowing a choice of selected bandwidth in the range of 0.5 nm to 4 nm, was used to record the UV-Vis absorbance scan of prepared nanomaterial. Luminescence spectrometer, having a source of xenon flash lamp laser in the range from 200 nm to 900 nm, was employed to examine the optical emission processes in prepared nanoparticles. We used InVia Raman microscope consisting of Ar^+ ion laser with 514.5 nm wavelength and 50 mW power, to record Raman spectrum of sample material.

3. Results and discussion

3.1. XRD analysis

We used Shimadzu XRD-6000 diffractometer for XRD analysis. The XRD crystallographic analysis helped us to determine the phase(s) present (peak position), concentration of phases (peak height), amorphous content (background bump) and crystallite size/strain (peak width) for prepared material [29]. The XRD pattern of the powder form of the sample was recorded and shown in Fig. 2.

The XRD pattern shows a single phase of ZCFO. The XRD peaks of ZCFO spinel phase correspond to planes (2 2 0), (3 1 1), (2 2 2), (4 0 0), (4 2 2), (5 1 1), (4 4 0). This is in good agreement with the values of JCPDS Card No. 82-1042, hence, formation of cubic phase of spinel ZCFO is confirmed. Having ascertained the single phase of ZCFO, we analyzed the remaining parameters of XRD peaks. No other peak, due to impurity or residual material, was observed.

The lattice constant (a = b = c) could be calculated from the most prominent peaks [9]. The Debye-Scherrer formula was used to determine the crystallite size D of ZCFO nanoparticles. The lattice strain was calculated from relation $\epsilon = \beta/\tan\theta$ [10], where β (radians) stands for full width at half maxima (FWHM) at a particular diffraction angle θ. The strain corresponding to each phase was calculated and shown in Table 1.

The crystallite size, the lattice constants, and lattice strain for ZCFO nanoparticles prepared by EWT approach are presented in Table 1. The crystallite size of ferrite nanoparticles is in the range of 1.8 nm to 12.5 nm. The average crystallite size and lattice constant were found to be 6.5 nm and 8.38 Å, respectively. The lattice strain developed in prepared nanocrystalline material could be caused by the high energy explosive process of EWT method. In order to directly determine the lattice constant, size and distribution of nanoparticle, we performed SEM characterization.

3.2. SEM analysis

XL-Philips 20 scanning electron microscope at IUAC, Delhi, was used for SEM analysis. The SEM image of the material prepared by our method and shown in Fig. 3, was analyzed to examine the shape, size, and distribution of the particles.

On the basis of small crystallite size (as estimated through XRD analysis) and observation of small as well large size structures in SEM images, we infer that the nanoparticles of the size less than ~70 nm actually coalesce to form larger size agglomerates. Thus, irregular shape nanoparticles are observed in the scanning electron micrograph. Here, the grains of 100 nm to 200 nm are

Table 1. Structural parameters determined for ZCFO nanoparticles.

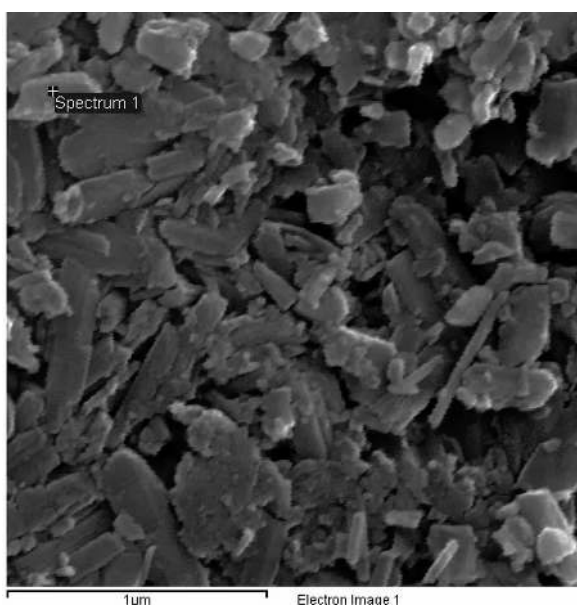| System	Angular positions [2θ°]	h k l	d-spacing [Å]	d-spacing (JCPDS) [Å]	D Crystal size [nm]	ε Lattice strain [%]	a = b = c [Å]	JCPDS [Å]
	30.4376	2 2 0	2.9656	2.9851	12.5	0.0105		
	35.6798	3 1 1	2.529	2.5457	06.0	0.0187		
ZCFO	37.4272	2 2 2	2.4214	2.4347	07.2	0.0151	8.388	8.443
nanoparticle	43.3048	4 0 0	2.097	2.1108	08.5	0.0110		
	53.7891	4 2 2	1.7121	1.7234	06.0	0.0127		
	57.6016	5 1 1	1.6142	1.6248	01.8	0.0404		
	62.6849	4 4 0	1.4828	1.4925	04.2	0.0157		

Fig. 3. Scanning electron micrograph of ZCFO.

observed. Porosity can also be seen at the interface of the grains. The high roughness of observed particles is usually related to high surface area and the ability to absorb gases, such as oxygen, could be harnessed. Therefore, pallets of ZCFO can actually be useful for gas sensing applications. Some researchers have demonstrated the application of ZCFO as LPG gas sensing material [10].

3.3. EDX analysis

EDX data were acquired in various regions of prepared nanomaterial and found to be the same as that of the region marked as "spectrum 1" in the SEM image (Fig. 3). Chemical composition of prepared nanomaterial on the basis of EDX spectrum shown in Fig. 4, is presented in Table 2. The existence of Zn, Cu, Fe, and O elements in Fig. 4 and Table 2 further endorses the formation of ZCFO nanoparticles.
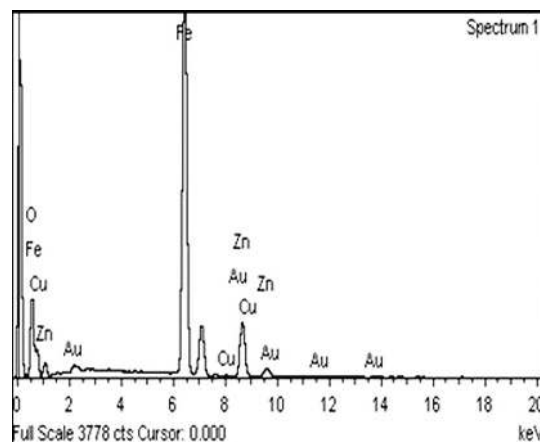

Fig. 4. EDX of the prepared nanoparticles.

Table 2. Quantitative estimation of constituent elements present in the sample.

Elements	O	Fe	Cu	Zn	Total
Weightage [%]	23.13	38.78	15.07	23.02	100

It can be concluded from EDX analysis that all basic constituents of ZCFO exist in the prepared nanomaterial, as revealed earlier by XRD characterization, as well.

3.4. FT-IR analysis

A PerkinElmer BX-II Fourier transform infrared spectrophotometer was used for FT-IR analysis. FT-IR spectroscopy is used for establishing the presence of functional groups in a molecule [32]. A typical signature of vibrational infrared spectrum extends from about 4000 cm^{-1} to 400 cm^{-1} [32]. In contrast to conventional IR spectroscopy, FT-IR spectroscopy uses all the frequencies simultaneously and their respective absorption frequencies are separated using mathematical Fourier transform [30].
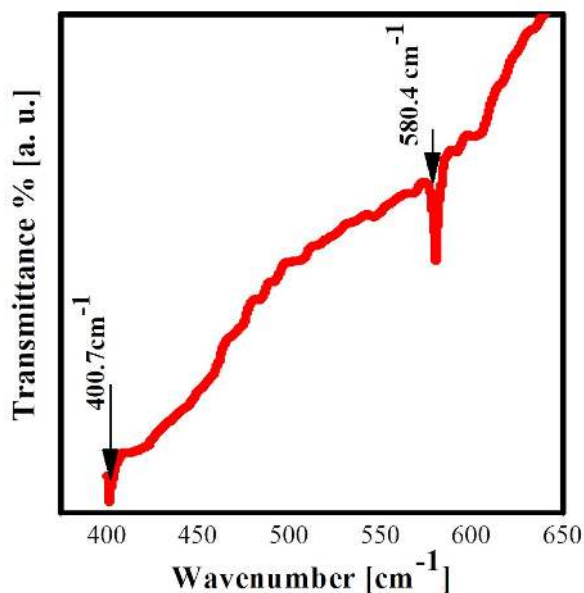

Fig. 5. FT-IR spectrum of ZCFO nanoparticles.

As shown in Fig. 5, two absorption bands of FT-IR spectrum, one at 400.7 cm^{-1} and the other one at 580.4 cm^{-1} are observed. The first band at 400.7 cm^{-1} confirms the formation of cation-oxygen bonds in octahedral sites and the second band at 580.4 cm^{-1} indicates the formation of metallic ion-oxygen bonds in tetrahedral sites [1]. The absorption spectroscopy of FT-IR, thus, confirms the spinel structure of the ferrite nanoparticles, as identified earlier through XRD analysis.

3.5. UV-Vis analysis

PerkinElmer Lambda 35 UV-Vis spectrophotometer was used for UV-Vis analysis. The analysis

of the absorption spectrum reveals the information about the band structure of any semiconductor material. The band gap of semiconductor can also be estimated by fundamental laws of absorption. The absorption coefficient of direct band gap semiconductor is given by Tauc relation:

$$(\alpha h \nu)^2 = A(h\nu - E_g) \tag{1}$$

where A is a constant. Adopting this equation, the absorption edge is extrapolated as the slope of linear plot of $(\alpha h\nu)^2$ versus $h\nu$. The extrapolated intercept on $h\nu$ axis gives the value of energy band gap E_g of nanoparticles and the same is shown as the inset of Fig. 6 [31, 33].
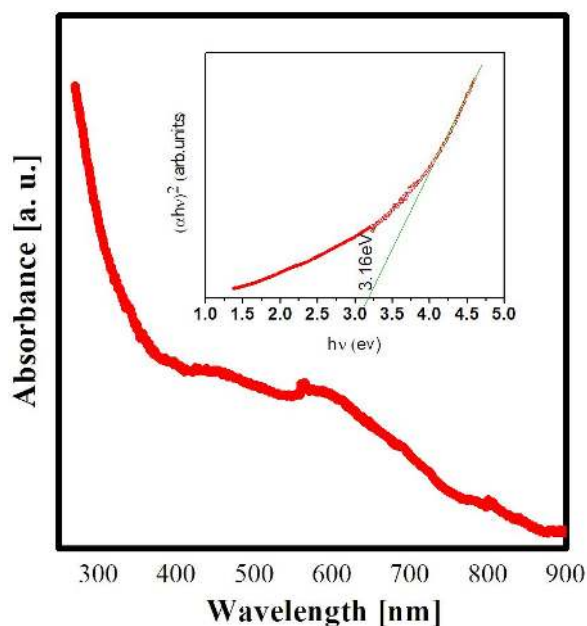

Fig. 6. UV-Vis absorption spectrum of synthesized nanoparticles. Plot of $(\alpha h\nu)^2$ vs. $h\nu$ is shown in the inset.

The value of band gap energy E_g of ZCFO nanoparticles was estimated to be 3.16 eV. Here, the optical absorption is significant in the 400 nm to 700 nm region. In line with previous reports, this indicates the blue shift in the value of absorption energies of prepared nanoparticles, arising basically due to size confinement effect [34]. On the basis of quantum mechanical consideration of particles in a box, it is a well-known concept that depending on the dimensionality of nanostructures

(i.e. 0-, 1- or 2-dimensional nanostructures) quasi-particles (e.g., electrons, holes, excitons, etc.) have confined motion and, consequently, the separation between energy levels is enhanced for nanostructures as compared to their bulk counterpart. Subsequently, the values of absorption and emission energies are enhanced for nanostructures. The dominant radiative absorption in 400 nm to 700 nm region could be due to interband absorption taking place amongst discrete energy states of valence and conduction bands [34–36]. Since ZCFO nanoparticles prepared by us have a wide range of the size variation from 1.8 nm to 12.5 nm, they exhibit a broad absorption region originating from different energy states. Thus, quantum size confinement in ZCFO nanoparticles, due to existence of discrete energy states and related blue shift in absorption energy, can be concluded. The blue shift in the band gap energy, as observed in UV-Vis spectrum, could be explicated by joint effect of following two phenomena. Firstly, the sp-d exchange interaction between valence band electrons of O and d electrons of Zn/Fe atoms [37]. Secondly, Burstein-Moss band filling effect caused by Fe atoms [37]. Widening of band gap region may lead to various defects and discrete energy states, therefore, it is of immense significance to examine the radiative recombination transitions occurring in prepared nanomaterial. Taking this into account, we performed fluorescence spectroscopy of present sample.

3.6. FL analysis

A PerkinElmer LS-55 luminescence spectrometer, Germany, was used for FL analysis. FL emissions for nanomaterials, synthesized by EWT are shown in Fig. 7.

The most intense FL peak is observed at 392 nm ($\sim$3.16 eV) corresponding to band gap transitions in UV region, which is just complementary to the absorption process observed in UV-Vis spectroscopy, as discussed before. Since our sample consists of multiple bonds (Fe–O, Zn–O, and Cu–O), we observe a wide band of visible emission spectra in the range of 500 nm to 600 nm. The center of this broad hump at 550 nm actually
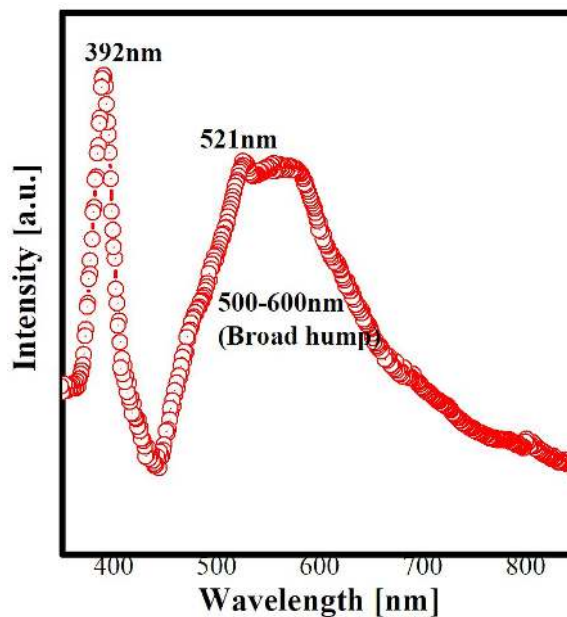
Fig. 7. FL spectra of the prepared nanomaterial.

corresponds to green-red emission. It was earlier established that the fluorescence of Fe doped ZnO nanoparticle at 521 nm corresponds to green emission [38]. The green-orange emission in the range of 500 nm to 600 nm is attributed to doubly ionized oxygen vacancies (O^{-2}) which trap the photogenerated holes [39]. Therefore, FL study endorses the formation of ZCFO, consisting of Fe–O, Zn–O, and Cu–O bonds, through present EWT based approach.

3.7. Micro-Raman analysis

Raman spectroscopy is one of the most efficient techniques to study the microstructure, crystallinity, disorder/distortion, and strain via investigation of polarizability changes in a material. In-Via Raman microscope from Renishaw UK system was used for micro-Raman analysis. In present case, inverse spinel structure of ZCFO could be confirmed by Raman analysis. The mixed ferrite $Fe^{+3}Zn^{+2}(Cu^{+2}Fe^{+3})O_4$ is a typical inverse spinel ferrite AB_2O_4, as A-sites are filled by Fe^{+3} and Zn^{+2} ions, whereas B-sites are occupied by equal number of Cu^{+2} and Fe^{+3} ions [9, 40]. As stated before, its crystalline structure belongs to cubic space group Fd3m (O_h^7) [41]. Oxygen atoms

form a close-packed face centered cubic (FCC) unit cell [40]. The metal ions (Zn^{+2}, Cu^{+2}, and Fe^{+3}) occupy stable tetrahedral A (8a) and octahedral B (16d) sites coordinated with respect to oxygen atoms [40]. Due to suitable fit of charge distribution of Cu^{+2} ions in the crystal field of octahedral sites, Cu^{+2} ions occupy octahedral sites [9]. Because of the sp^3 hybrid orbitals formation, Zn^{+2} can form covalent bonds, therefore, occupy tetrahedral sites [42]. Moreover, Cu^{+2} has smaller radius (0.69 Å) as compared to the one of Zn^{+2} (0.74 Å). The cation distribution in a cubic spinel system usually plays a vital role in magnetic properties of ZCFO. Even magnetic properties vary in accordance with the distribution of Zn^{+2} and Cu^{+2} in interstitial, tetrahedral and octahedral sites. This distribution of cations is highly dependent on synthesis technique.
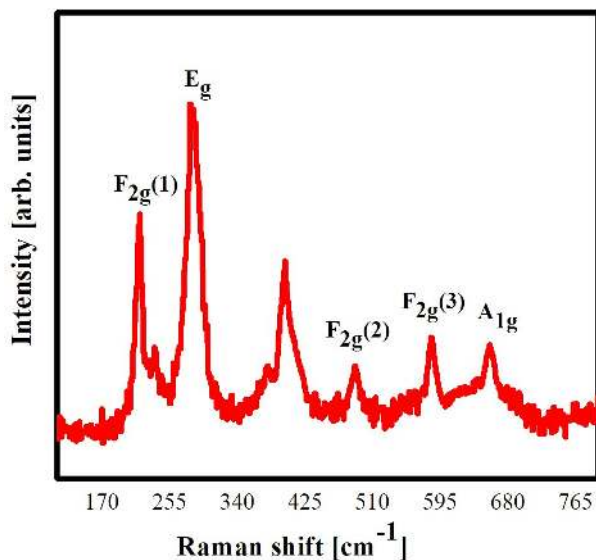

Fig. 8. Raman spectrum of ZCFO nanoparticles along with the prominent modes assignment.

Raman spectroscopy analysis efficiently reveals the cation distribution in a cubic spinel system [43]. According to classical group theory, the modes of cubic spinel structure, belonging to the space group Fd3m, are as follows: $\Gamma = A_{1g}(R) + E_g(R) + F_{1g} + 3F_{2g}(R) + A_{2u} + 2E_u + 4F_{1u}(IR) + 2F_{2u}$. Here, A_{1g}, E_g, and $3F_{2g}$ are first order Raman active

modes [40, 44]. The $4F_{1u}$ modes are IR active [40, 44]. F_{1g}, A_{2u}, $2E_u$, and $2F_{2u}$ are silent modes [45–47]. The unpolarized Raman spectrum of prepared nanomaterial is presented in Fig. 8.

As it can be seen in Fig. 8 and also in Table 3, all the five expected phonon bands are located at 222 cm^{-1}, 290 cm^{-1}, 494 cm^{-1}, 689 cm^{-1} and 661 cm^{-1} for obtained nanoferrite phase. The modes around 410 cm^{-1} to 420 cm^{-1} and 1322 cm^{-1} are characteristic signatures of hematite corresponding to $E_g(u)$ mode [40]. The peak at 405 cm^{-1}, earlier investigated extensively for magnetite properties, is observed due to experimental process involved with Raman spectroscopy [40]. The laser used in the experiment has been focused on a few μm spot in diameter and that led to a rise in temperature up to hundreds of degrees [40]. At such a high temperature, the powdered ferrite sample undergoes spontaneous oxidation, forming hematite [40]. Even small traces of hematite lead to observation of prominent modes in Raman spectrum [40].

Thus, the Raman data of present sample are in a good agreement with the data of inverse spinel ferrites presented in Table 4. Finally, from the present detailed Raman analysis, we comprehend that the used method of EWT leads to the formation of pure phase ZCFO nanoparticles and this is in a good agreement with XRD, UV, FL and FT-IR analysis, as discussed previously.

4. Conclusions

In summary, the synthesis of single phase ZCFO nanoparticles has been achieved through present facile, and cost-effective approach based on EWT. Structural, optical and vibrational properties of the prepared nanomaterial were revealed through detailed characterizations, as reported in the present work. The spinel structure of ZCFO nanoparticles along with crystallite size and lattice parameters was confirmed by XRD analysis. The presence of Fe–O, Zn–O, and Cu–O bonds was revealed by FT-IR analysis. Raman analysis confirmed that Cu and Fe cations occupy octahedral sites and their stretching bonds with O (oxygen)

Table 3. Comparison of present Raman modes with literature reports.

Literature	Raman shift [cm^{-1}]						
Present work	222	242	290	406	494	589	661
Graves et al. [48]	226	−	366	−	490	570	706
Gasparov et al. [49]	193	−	308	−	−	540	670
Dunnwald and Otto [50]	−	−	298	418	470	550	676
Verble et al. [51]^a	−	−	300	420		560	680
Hart et al. [52]	−	−	298	420	472	550	676
Degiorgi et al. [53]^b	160	−	318	410	462	542	672
Gupta et al. [54]	−	−	300	410	−	540	669
Bersani et al. [55]	−	−	311	−	−	541	666
de Faria et al. [56]	−	−	301.6	−	−	533.6	662.7
Ohtsuka et al. [57]	−	−	−	−	−	540	665
Boucherit et al. [58]	−	−	−	−	−	550	670
Thierry et al. [59]	−	−	−	−	−	550	670
Li et al. [60]	−	−	−	−	−	540	665
Wang Z. et al. [41]	221	242	355	−	451	−	647

^{a}at 77 K, ^{b}at 130 K

Table 4. Comparison of obtained Raman modes with some inverse spinel ferrites.

Ferrites	First order active modes and Raman shift [cm^{-1}]					
	$F_{2g}(1)$	E_g	$F_{2g}(2)$	$F_{2g}(3)$	A_{1g}	Literature
$ZnCuFe_2O_4$	222	242	290	494	589	661 Present work
$MgFe_2O_4$	217	–	333	486	554	715 [61]
$FeFe_2O_4$	193	–	306	–	538	668 [40]
$FeFe_2O_4$	226	–	336	490	570	706 [48]
$NiFe_2O_4$	–	–	339	490	579	700 [48]
$MnFe_2O_4$	–	–	331	496	543	625 [48]

vibrate at lower frequencies, whereas Zn and Fe occupy tetrahedral sites and their stretching bonds with O (oxygen) vibrate with higher frequency. Hence, it was established that prepared nanoferrites have inverse spinel structure. Furthermore, the presence of Cu cation, having smaller ionic radius as compared to that of Zn cation, causing the inversion, was confirmed through the present Raman analysis. ZCFO nanoparticles prepared by us are optically active as demonstrated through UV-Vis absorption and fluorescence spectroscopic analyses, hence, could be a potential candidate for gas sensing applications.

References

[1] THAKUR P., SHARMA R., KUMAR M., KATYAL S.C., NEGI N.S., THAKUR N., *Mater. Res. Express*, 3 (2016), 75001.

[2] LOPEZ J., GONZALEZ-BAHAMON L.F., PRADO J., CAICEDO J.C., ZAMBRANO G., GOMEZ M.E., ESTEVE J., PRIETO P., *J. Magn. Magn. Mater.*, 324 (2012), 394.

[3] Ghasemi A., Hossienpour A., Morisako A., Saatchi A., Salehi M., *J. Magn. Magn. Mater.*, 302 (2006), 429.

[4] Komarneni S., Fregeau E., Breval E., Roy R., *J. Am. Ceram. Soc.*, 71 (1988), C26.

[5] Hrianka I., Malaescu I., *J. Magn. Magn. Mater.*, 150 (1995), 131.

[6] Wang C., Zhang X.M., Qian X.F., Xie J., Wang W.Z., Qian Y.T., *Mater. Res. Bull.*, 33 (1998), 1747.

[7] Yamamoto Y., Makino A., *J. Magn. Magn. Mater.*, 133 (1994), 500.

[8] Kodama R.H., Berkowitz A.E., McNiff Jr. E.J., Foner S., *Phys. Rev. Lett.*, 77 (1996), 394.

[9] Banerjee M., Verma N., Rasad R., *J. Mater. Sci.*, 42 (2007), 1833.

[10] Jain A., Baranwal R.K., Bharti A., Vakil Z., Prajapati C.S., *Sci. World J.*, 2013 (2013), 790359.

[11] Jaswal L., Singh B., *J. Integr. Sci. Technol.*, 2(2) (2014), 67.

[12] Goswami N., Singh S., Katyal S.C., *J. Laser. Opt. Photonics*, 4 (2017) 158.

[13] Abdeen A.M., *J. Magn. Magn. Mater.*, 185 (1998), 199.

[14] Gubbala S., Nathania H., Koizolb K., Misra R.D.K., *Physica B*, 348 (2004), 317.

[15] Daliya S.M., Ruey-Shin J., *Chem. Eng. J.*, 129 (2007), 51.

[16] Toledo J.A., Valenzuela A., Bosch P., Amendariz H., Montoya A., Nova N., Vazquez A., *Appl. Catal. A-Gen.*, 198 (2000), 235.

[17] Radheshyam A., Dwivedi R., Reddy V.S., Charry K.V.R., Prasad R., *Green Chem.*, 4 (2002), 558.

[18] Sreekumar K., Mathew T., Devassy B.M., Rajgopal R., Vetrivel R., Rao B.S., *Appl. Catal. A-Gen.*, 20 (2001), 11.

[19] Pannaparayil T., Komarneni S., Marande R., Zardrho M., *J. Appl. Phys.*, 67 (1990), 5509.

[20] Zhao W., Fang M., Wu F., Wu H., Wang L. Chen G., *J. Mater. Chem.*, 20 (2010), 5817.

[21] Ramesh S., *J. Nanosci. Nanotechno.*, 2013 (2013), 929321.

[22] Goswami N., Sen P., *Solid State Commun.*, 132 (2004), 791.

[23] Goswami N., Sen P., *J. Nanopart. Res.*, 9 (2007), 513.

[24] Goswami N., Sen P., *Mater. Res. Express*, 1 (2014), 25001.

[25] Sahai A., Goswami N., Kaushik S.D., Tripathi S., *Appl. Surf. Sci.*, 390 (2016), 974.

[26] Goswami N., Sen P., *Appl. Surf. Sci.*, 425 (2017), 576.

[27] Yamauchi S., Goto Y., Hariu T., *J. Cryst. Growth*, 260 (2004), 1.

[28] Siwach O.P., Sen P., *J. Nanopart. Res.*, 10 (2008), 107.

[29] Kaufmann E.N., *Characterization of Materials*, John Wiley & Sons, Inc., Hoboken, New Jersey, 2003.

[30] Sahai A., Goswami N., *Physica E*, 58 (2014), 130.

[31] Zeng H., Cai W., Li Y., Hu J., Liu P., *J. Phys. Chem. B*, 109 (2005), 18260.

[32] Sahai A., Kumar Y., Agarwal V., Olive-Mendez S.F., Goswami N., *J. Appl. Phys.*, 116 (2014), 164315.

[33] Pankove J.I., *Optical Processes in Semiconductors*, Dover, New York, 1971.

[34] Goswami N., Sharma D.K., *Physica E*, 42 (2010), 1675.

[35] Hu Y., Chen H.J., *J. Nanopart. Res.*, 10 (2008), 401.

[36] Madelung O., *Semiconductors: Data Handbook*, Springer, New York, 2004.

[37] Kumar S., Mukherjee S., Singh R.K., Chatterjee S., Ghosh A.K., *J. Appl. Phys.*, 110 (2011), 103508.

[38] Srivastava A.K., Deepa M., Bahadur N., Goyat M.S., *Mater. Chem. Phys.*, 114 (2099), 194.

[39] Dijken A.V., Meulenkamp E., Vanmaekelbergh D., Meijerink A., *J. Lumin.*, 90 (2000), 123.

[40] Shebanova O.N., Lazor P., *J. Solid State Chem.*, 174 (2003), 424.

[41] Wang Z., Schiferl D., Zhao Y., O'Neill H.ST.C., *J. Phys. Chem. Solids*, 64 (2003), 2517.

[42] Gonzalez-Angeles A., Mendoza-Suarez G., Gruskova A., Papanova M., Slama J., *Mater. Lett.*, 59 (2005), 26.

[43] Saikiaa K., Kaushikb S.D., Sen D., Mazumder S., Deb P., *Appl. Surf. Sci.*, 379 (2016), 530.

[44] Romcevic N., Kostic R., Romcevic M., Hadzic B., Kudelska I.K., Dobrowolski W., Narkiewicz U., Sibera D., *Acta Phys. Pol. A*, 114 (2008), 1323.

[45] Damen T.C., Porto S.P.S., Tell B., *Phys. Rev.*, 142 (1966), 570.

[46] Arguello C.A., Rousseau D.L., Porto S.P.S., *Phys. Rev.*, 181 (1969), 1351.

[47] Goswami N., Sahai A., *Mater. Res. Bull.*, 48 (2013), 346.

[48] Graves P.R., Johnston C., Campaniello J.J., *Mater. Res. Bull.*, 23 (1988), 1651.

[49] Gasparov L.V., Tanner D.B., Romero D.B., Berger H., Margaritondo G., Forro L., *Phys. Rev. B*, 62 (2000), 7939.

[50] Dunnwald J., Otto A., *Corros. Sci.*, 29 (1989), 1167.

[51] Verble J.L., *Phys. Rev. B*, 9 (1974), 5236.

[52] Hart T.R., Adams S.B., Tempkin H., Balkanski M., Leite R., Porto S., *Proc. Inter. Conf. Light Scatter. Sol.*, (1976), 254.

[53] Degiorgi L., Blatter-Mörke I., Wachter P., *Phys. Rev. B*, 35 (1987), 5421.

[54] Gupta R., Sood A.K., Metcalf P., Honig J.M., *Phys. Rev. B*, 65 (2002), 104430.

[55] Bersani D., Lottici P.P., Montenero A., *J. Raman Spectrosc.*, 30 (1999), 355.

[56] de Faria D.L.A., Silva S.V., de Oliveira M.T., *J. Raman Spectrosc.*, 28 (1997), 873.

[57] OHTSUKA T., KUBO K., SATO N., *Corrosion-US*, 42 (1986), 476.

[58] BOUCHERIT N., GOFF A.H., JOIRET S., *Corros. Sci.*, 32 (1991), 497.

[59] THIERRY D., PERSSON D., LEYGRAF C., BOUCHERIT N., GOFF A.H., *Corros. Sci.*, 32 (1991), 273.

[60] LI J.M., HUAN A.C.H., *Phys. Rev. B*, 61 (2000), 6876.

[61] WANG Z., LAZOR P., SAXENA S.K., O'NEILL H.S.C., *Mat. Res. Bull.*, 37 (2002), 1589.